Synthesis and Characterization of Silver-Coated Graphite Nanosheets with Pyrrole via *In Situ* Polymerization

Yongqing Yang, Shuhua Qi, Yunchuan Qin, Xinxin Zhang

Department of Applied Chemistry, School of Science, Northwestern Polytechnical University, Xi'an 710072, People's Republic of China

Received 3 July 2011; accepted 17 August 2011
DOI 10.1002/app.36383
Published online 20 January 2012 in Wiley Online Library (wileyonlinelibrary.com).

ABSTRACT: Polypyrrole (PPy)/graphite nanosheet (NanoG) and PPy/silver-coated graphite nanosheet (Ag/NanoG) nanocomposites were synthesized via *in situ* polymerization with the monomer Py polymerized on the surface of NanoGs and Ag/NanoGs. The morphologies and nanostructures of NanoGs, Ag/NanoGs, PPy, PPy/NanoG, and PPy/Ag/NanoG were characterized by scanning electron microscopy, Fourier transmission infrared spectroscopy, and X-ray diffraction analysis. The results showed that most of NanoG and Ag/NanoG nanoparticles were encapsulated by PPy for a layered structure and high aspect ratio (width-to-thickness ratio) of NanoGs and Ag/NanoGs. From the thermogravimetric analysis, we observed that the introduction of inorganic nanosilver and NanoGs into the composites made the composites exhibit a better thermal stability than pure PPy. According to the four-point probe test, the conductivities of the ultimate PPy/NanoG and PPy/Ag/NanoG composites increased dramatically compare to that of pure PPy. The measurement of electromagnetic parameters showed that the reflection loss of PPy/Ag/NanoG was below −15 dB at an *X* band from 8.2 to 12.4 GHz, and the minimum loss value was −18.21 dB at 9.86 GHz. The reflection loss of PPy/NanoG was below −10 dB at an *X* band from 8.2 to 12.4 GHz, and the minimum loss value was −13.44 dB at 10.28 GHz. The microwave-absorbing properties of PPy/Ag/NanoG and PPy/NanoG were superior to those of PPy. © 2012 Wiley Periodicals, Inc. J Appl Polym Sci 125: E388–E397, 2012

Key words: conducting polymers; microstructure; nanocomposites

INTRODUCTION

In recent years, polymer-based conducting composites containing electrical nanoparticles have been of special interest because of their unique electrical properties and potential applications in a wide range of fields, including Electro Magnetic Interference (EMI) shielding, catalysis, capacitors, rechargeable batteries, conductive inks, antistatic textiles, and secondary batteries. Polymers with conjugated double bonds in their chains, such as polyacetylene, polypyrrole (PPy), polyaniline, and polythiophene, have been deeply investigated.[1–5] Among these conducting polymers, PPy has attracted much attention for its many predominant properties, including it multiple electronic states, high conductivity upon doping, easy and economic preparation, and good environmental stability.[6] However, its conductivity and microwave-absorbing properties are still low. To improve its properties, conductive materials, such as carbon black,[7] carbon fibers,[8] graphene,[9] and carbon nanotubes,[10] have often been filled into it. Nowadays, much attention has been paid to graphite because of its unique mechanical, chemical, and electrical properties.[11–13]

Graphite is well known to be a layered material with a high conductivity that can be intercalated by chemical reagents such as nitric acid(HNO_3) or sulfuric acid(H_2SO_4) and can form another kind of compound called *graphite intercalation compounds* (GICs). GICs tend to be more electrically conductive than graphite because of the charge transfer between the intercalate and graphite. By rapid thermal treatment, GICs can be expanded to several hundreds times their original volume to get expanded graphite (EG).As a conductive filler, much work has been done on polymer/EG materials.[14–16]

In this article, graphite nanosheets (NanoG) were prepared by ultrasonication of EG in an aqueous alcohol solution. The high aspect ratio (width-to-thickness ratio) of NanoG leads to its high conductivity. To further improve the electronic properties of the composites, nanometal is usually chemically coated on the surface of the inorganic materials.[17–20] Among the metals, Ag was chosen for its good conductivity and stability. The aim of this study was to fabricate the nanocomposites via the *in situ* polymerization of pyrrole (Py) in the presence of NanoG and silver-coated graphite nanosheets (Ag/NanoG). The morphologies and nanostructures of NanoG, Ag/NanoG, PPy/NanoG, and PPy/Ag/NanoG were characterized by scanning electron microscopy (SEM), energy-dispersive spectroscopy (EDS), Fourier transform infrared (FTIR)

Correspondence to: Y. Yang (ylqqyyq@yahoo.cn).

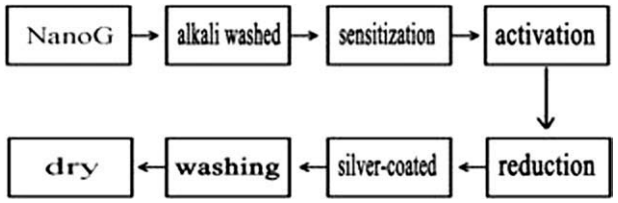

Figure 1 Preparation of Ag/NanoG.

spectroscopy, and X-ray diffraction (XRD). Their properties, including their thermal stability, conductivity, and microwave absorbance, were studied.

EXPERIMENTAL

Materials

The oxidized graphite (OG) was supplied by Shandong Qingdao Graphite Co. (Qingdao, China). Py (analytical reagent) was bought from Sinopharm Chemical Reagent Limited Co. (Shanghai, China) and was distilled under reduced pressure before use. Ferric chloride ($FeCl_3{\cdot}6H_2O$), palladium chloride ($PdCl_2$), and tin chloride dihydrate ($SnCl_2{\cdot}2H_2O$) were bought from Chemical Company of Tianjin (Tianjin, China). Formaldehyde (HCHO), 36% hydrochloric acid (HCl), sodium hydroxide (NaOH), ammonia ($NH_3{\cdot}H_2O$), silver nitrate ($AgNO_3$), KH550, and ethanol (analytical grade) were bought from Chemical Company of Xi'an (Xi'an, China).

Synthesis of NanoG

NanoG was prepared from OG by two steps. OG was subjected to a thermal expansion at 900–1000°C for 15 s in a muffle furnace to form EG. Then, the EG was immersed in an aqueous solution containing 70% alcohol and 30% distilled water and exfoliated in an ultrasonic bath for 24 h. The product was then filtered, washed, and dried in a vacuum at 80°C for about 8 h to get NanoG. The preparation processes of NanoG were as follows:

$$\text{oxidized graphite (OG)} \xrightarrow{900\sim1000^{\circ}\text{C, 15s}} \text{expanded graphite (EG)} \xrightarrow{\text{ultrasonic}} \text{NanoG}$$

Synthesis of Ag/NanoG

The preparation of Ag/NanoG involved an initial pretreatment of NanoG and a subsequent reduction of $AgNO_3$ in the presence of HCHO (Fig. 1).

Surface treatment of NanoG

Three steps, alkali washing, sensitization, and activation, were used to pretreat NanoG. NanoG (1 g) was first alkali-washed in 50 mL of an NaOH (10%) solution for about 1 h to get rid of impurities and was then sensitized by 0.5 g of $SnCl_2{\cdot}2H_2O$ for about 0.5 h. After that, the sensitized NanoGs was activated by 0.025 g of $PdCl_2$ to enhance the adhesion force between the silver coating and NanoGs. The reaction of $SnCl_2{\cdot}2H_2O$ and $PdCl_2$ was as follows:[21]

$$Sn^{2+} + Pd^{2+} = Sn^{4+} + Pd$$

The obtained Pd was used as a catalyst in the following procedure.

Synthesis of Ag/NanoG

After pretreatment, 1 g of NanoG was treated by ultrasonication for 30 min and then discharged into a three-necked, round-bottom flask with a mixture of $AgNO_3$ (3.4 g), $NH_3{\cdot}H_2O$, malic acid, and distilled water. The mixture was stirred for 30 min, and the pH value was kept at 8–9. Then, the reducing agent HCHO was added to the flask drop by drop. The mass ratio of $AgNO_3$ to HCHO was about 4. The reaction was carried out at room temperature for 1 h. After the reaction, 1 mol/L NaOH was used to adjust the pH to the range 10.5–11. Then, the suspension was altered, washed several times with distilled water, and dried in an oven at about 80°C. The reaction was as follows:

$$HCHO + 4[Ag(NH_3)_2]OH \rightarrow 4Ag\downarrow + 6NH3\uparrow + (NH_4)_2CO_3 + 2H_2O$$

Synthesis of PPy

PPy was prepared by the following procedure.[22] A mixture of ethanol, distilled water, and 1*M* HCl solution was added to a three-necked, round-bottom flask with stirring. Then, an amount of Py was added to the flask, which was kept in an ice–water bath. After the temperature of the mixture fell below 5°C, a solution of $FeCl_3{\cdot}6H_2O$ was added dropwise into the mixture; the mass ratio of Py to $FeCl_3{\cdot}6H_2O$ was about 1 : 5. The reaction was carried out for about 6 h, and the pH value was kept at 2–4. The color of the mixture changed from yellow green to dark green. The resulting precipitate was filtered, washed with distilled water and ethanol repeatedly, and dried *in vacuo* at 60°C for about 24 h.

Synthesis of the PPy/NanoG and PPy/Ag/NanoG nanocomposites

PPy/NanoG was prepared by *in situ* polymerization. An amount of NanoG was added to the KH550 solution and dispersed by ultrasonication for about 1 h.

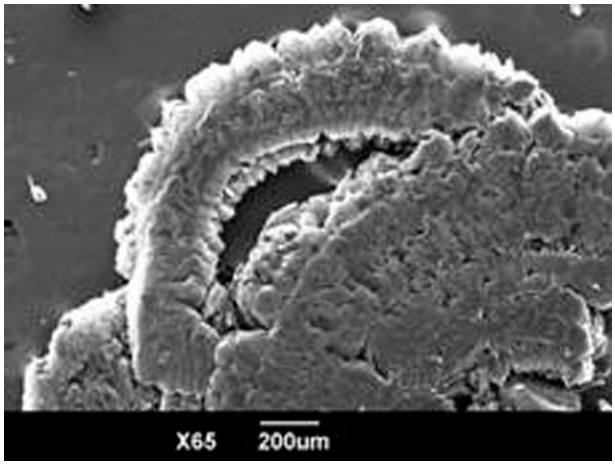

Figure 2 SEM image of EG.

After filtration and washing with distilled water, the pretreated NanoG and a mixture of ethanol, distilled water, and 1*M* HCl solution were discharged into a three-necked, round-bottom flask with stirring. The mixture was sonicated for 1 h. Then, Py was added to the flask, which was kept in an ice–water bath. After the temperature of the mixture fell below 5°C, a solution of $FeCl_3{\cdot}6H_2O$ was added dropwise into the mixture; the mass ratio of Py to $FeCl_3{\cdot}6H_2O$ was about 1 : 5. The reaction was carried out for 6 h. The color of the mixture changed from yellow green to dark green. The resulting precipitate was filtered, washed with distilled water and ethanol repeatedly, and dried *in vacuo* at 60°C for about 24 h.

The PPy/Ag/NanoG nanocomposite was synthesized by *in situ* polymerization as discussed previously.

Characterization

The structures of NanoG, Ag/NanoG, PPy, PPy/NanoG, and PPy/Ag/NanoG were characterized with SEM (JSM-6390, Hitachi, Tokyo, Japan), EDS analysis (JED-2200 Series, Tokyo, Japan), FTIR spectroscopy (WQF-510, Ruili, Beijing, China), and XRD (PANalytical, Amsterdam, Holland), respectively.

The conductivities of NanoG, Ag, and the Ag/NanoG, PPy, PPy/NanoG, and PPy/Ag/NanoG nanocomposites were measured with an SZ-82 digital four-probe resistance tester (Suzhou Electronic Equipment Factory, China). For the measurement of electrical properties, circle samples with a diameter of 15 mm and a thickness of 2 mm were prepared by casting into the stainless forms and cold-pressed. The thermal properties of PPy and the PPy/NanoG and PPy/Ag/NanoG nanocomposites were analyzed with thermogravimetric (TG) analysis (SDT-2960, State of Delaware, US) at a heating rate of 10°C/min in the range 20–800°C under a nitrogen atmosphere. The electromagnetic parameters were analyzed with an HP8753D vector network analyzer (California, US) and the samples were $22.86 \times 10.16 \times 2$ mm^3.

RESULTS AND DISCUSSION

SEM and EDS analyses

To investigate the morphology of the as-prepared sample in detail, the obtained samples, including EG, NanoG, PPy, and the Ag/NanoG, PPy/NanoG, and PPy/Ag/NanoG nanocomposites were characterized with SEM.

SEM of EG, NanoG, and Ag/NanoG

Usually, EG is prepared from OG, which is subjected to a thermal expansion at 800–1000°C for 15 s in a muffle furnace; it can expand many times its original volume with heat treatment. The structure of EG could be clearly characterized by SEM (shown in Fig. 2). It could be seen that EG had a wormlike shape and consisted of numerous parallel nanosheets.[23] By expansion, the layered structure of EG deformed in an irregular pattern and formed a network structure that consisted of many pores of different sizes ranging from the microscale to the nanoscale.[24,25]

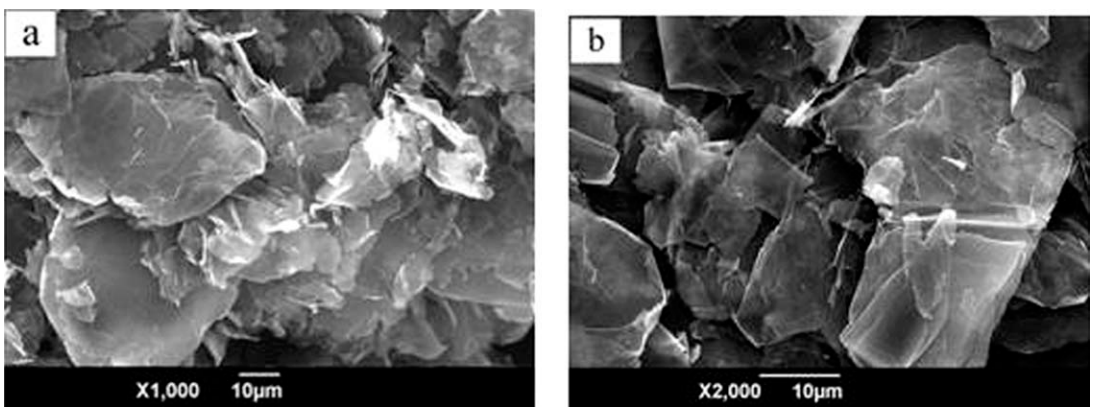

Figure 3 SEM images of NanoG.

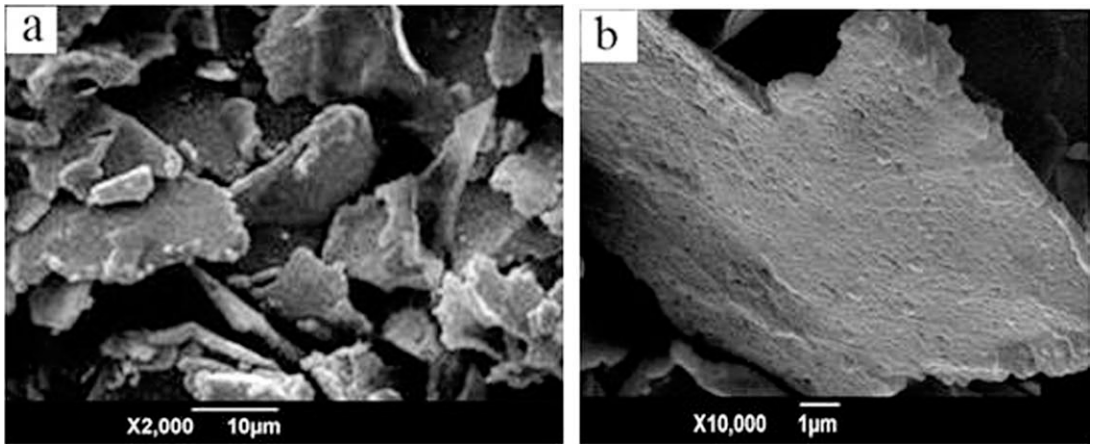

Figure 4 SEM images of Ag/NanoG.

SEM of NanoG

By treating the EG with ultrasonication in an aqueous solution of 70% ethanol and 30% distilled water, the inorganic material NanoG was prepared. Figure 3 shows the SEM micrograph of NanoG. It can be seen that the EG was efficiently exfoliated to ultrathin, transparent NanoG with a width ranging from 1 to 20 μm and a thickness ranging from 30 to 90 nm; this indicated a large aspect ratio (width-to-thickness ratio) of the NanoG. The higher the aspect ratio (width-to-thickness ratio) of the material was, the lower the filler content was, and the higher the electrical conductivity was.

SEM of Ag/NanoG

Ag/NanoG is usually prepared by a chemical reaction between the oxidant $AgNO_3$ and the reductant HCHO on the surface of NanoG. The SEM images of Ag/NanoG at magnifications of 2000 and 10,000× are shown in Figure 4. It can be seen that NanoG was fully covered with Ag nanoparticles. Most of the nanosilver particles were connected with each other on the surface of NanoG. The thickness of Ag/NanoG was about 200 to 250 nm.

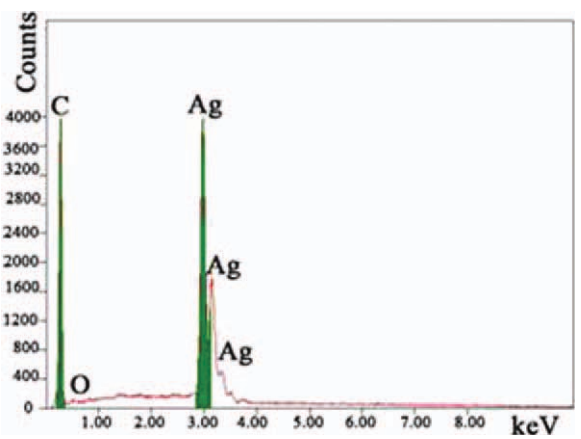

Figure 5 EDS of Ag/NanoG. [Color figure can be viewed in the online issue, which is available at wileyonlinelibrary.com.]

EDS of Ag/NanoG

Elements and their quantities of Ag/NanoG were measured by EDS analysis. Figure 5 confirms the presence of C, Ag, and O in Ag/NanoG. The mass content of Ag in Ag/NanoG could reach 74.80%; this further reflected the coating of C by Ag (Table I). The small amount of O came from the functional groups of —OH and —COOH on the NanoG surface. Other O may have come from the oxidization of Ag by air.

SEM of PPy, PPy/NanoG, and PPy/Ag/NanoG

PPy was prepared by *in situ* polymerization, and its structure was clearly characterized by SEM images. Figure 6 shows that the PPy particles appeared to be spherical in shape and connected with each other in ethanol by hydrogen bonds between them. Their diameter could reach the nanometer grade. Figures 7 and 8 show the surface morphologies of PPy/NanoG and PPy/Ag/NanoG, respectively. It could be seen that there were lots of small bright nanoparticles on the surface of NanoG and Ag/NanoG. Inorganic NanoG and Ag/NanoG were wrapped up by PPy. During the *in situ* polymerization, NanoG and Ag/NanoG were pretreated with KH550. After

TABLE I
Elements Analyses of Ag/NanoG

Elements	keV	Mass (%)	Error (%)	Atom (%)
C K	0.277	22.47	0.05	68.90
O K	0.525	2.73	0.18	6.26
Ag L	2.983	74.80	0.69	24.84
Total		100.00		100.00

K, K shell electron; L, L shell electron

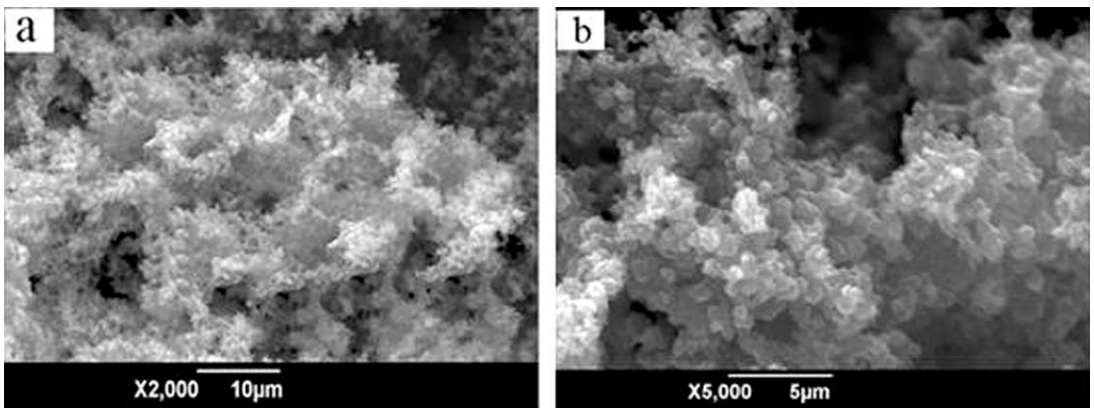

Figure 6 SEM images of PPy.

hydrolysis, KH550 could produce methylsilane functional groups, which connected the inorganic fillers with PPy. At the same time, hydrogen bonds were formed between —H provided by PPy and —OH provided by NanoG and Ag/NanoG. NanoG and Ag/NanoG were used as hard templates; thus, Py could easily react on the surface of NanoG and Ag/NanoG. The flakelike structure of NanoG and Ag/NanoG restrained the PPy chains from tangling with each other, so the dispersity of the composites was superior to PPy.

XRD analysis

XRD analyses of NanoG, Ag, and Ag/NanoG

The crystal structures of NanoG, Ag, and Ag/NanoG were characterized by XRD, and the results are shown in Figure 9. The peaks at $2\theta = 26.46$ and 55.64° corresponded to the (002) and (110) planes, respectively, and were the typical diffraction peaks of graphite (JCPDS file no. 75-1621). In Figure 9(b), another four diffraction peaks at 38.14, 44.28, 64.46, and 77.68° can be observed; these indicated the (111), (200), (220), and (311) planes of silver's cubic face-centered structure (JCPDS file no. 04-0783). In Figure 9(c), that is, the X-ray curve of Ag/NanoG, the typical planes of both graphite [(002) and (111)] and silver [(111), (200), (220), and (311)] were observed; these agreed well with earlier reports.[26–30] The diffraction peaks of Ag/NanoG were relatively weaker than those of NanoG and Ag, respectively. This indicated that the surface of NanoG was covered with silver particles, which weakened the diffraction peak strength of NanoG.

XRD analysis of PPy, PPy/NanoG, and PPy/Ag/NanoG

The crystal structures of PPy, PPy/NanoG, and PPy/Ag/NanoG were characterized by XRD, and the results are shown in Figure 10. Figure 10(a) shows the XRD pattern of PPy, which had a broad peak at $2\theta = 15$–30°. This indicated the amorphous behavior of the polymer. The broad peak resulted from the X-ray scattering of the PPy chain. As is known, most of α–α′ bonds are formed during the *in situ* polymerization of Py by chemical oxidization. At the same time, some α–β bonds can also be formed that damage the sequence of the polymer chain and lead to the amorphous behavior of the polymer. Figure 10(b) shows the XRD pattern of PPy/NanoG. The peak at 26.46° corresponded to the

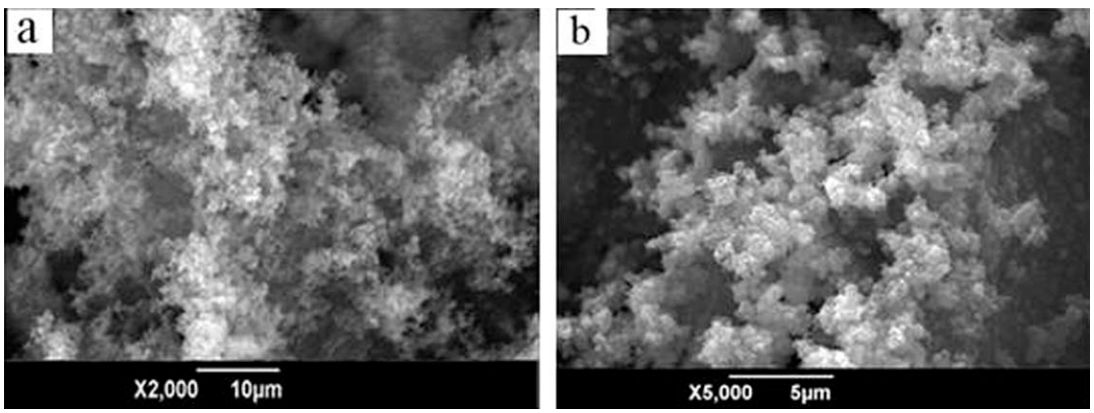

Figure 7 SEM images of the PPy/NanoG composite.

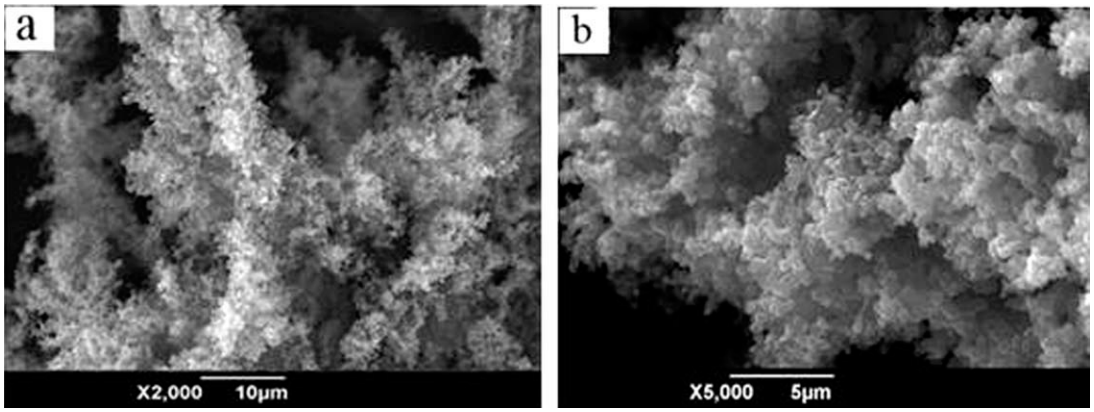

Figure 8 SEM images of the PPy/Ag/NanoG composite.

(110) plane and was a typical diffraction peak of graphite. A relatively weak broad peak was also seen at $2\theta = 15–30°$. Figure 10(c) shows the XRD pattern of PPy/Ag/NanoG. The typical planes of both graphite [(002)] and silver [(111), (200), (220), and (311)] were observed; this agreed well with earlier reports.

There were broad peaks in the all of the X-ray curves of PPy, PPy/NanoG, and PPy/Ag/NanoG. Among the three curves, the strength of the broad peaks in PPy/NanoG and PPy/Ag/NanoG were weaker than those of PPy. The addition of the inorganic filler had a great effect on the PPy, including on the doping degree, the force among the PPy chains within the structure, and the force between the PPy chains and the counter ion. This affected affect the strength of the diffraction peaks.

FTIR spectral analysis of PPy, PPy/NanoG, and PPy/Ag/NanoG

The FTIR spectra of pure PPy, PPy/NanoG, and PPy/Ag/NanoG are shown in Figure 11. All three samples had the typical structure of PPy, as shown in Figure 11(a). The band at 3427 cm^{-1} corresponded to the N—H stretching vibrations in the Py ring. The band at 1620 cm^{-1} related to the N—H in-plane deformation vibrations, and that at 1424 cm^{-1} reflected the C—N stretching vibrations. The =C—H in-plane deformation vibrations were situated at 1155 cm^{-1}, and the C—C stretching vibrations were seen at 1524 cm^{-1}. The out-of-plane deformation vibrations of the N—H and C—H were situated at 1022 and 885 cm^{-1}.These results indicate the formation of PPy by *in situ* polymerization. Figure 11(b,c) shows the FTIR spectra of PPy/NanoG and PPy/Ag/NanoG. Their wave numbers are shown in Table II. All of the typical structures of PPy could be seen in these two curves.

Compared with the FTIR spectrum of PPy, all of the bands of PPy/NanoG and PPy/Ag/NanoG showed a great blueshift; this indicated that the vibration and electron delocalization strength of the PPy chain changed after compounding with NanoG and Ag/NanoG. This was attributed to the small size effect and quantum size effect of the inorganic filler. During the formation of the composites, KH550 was used as the coupling agent and formed

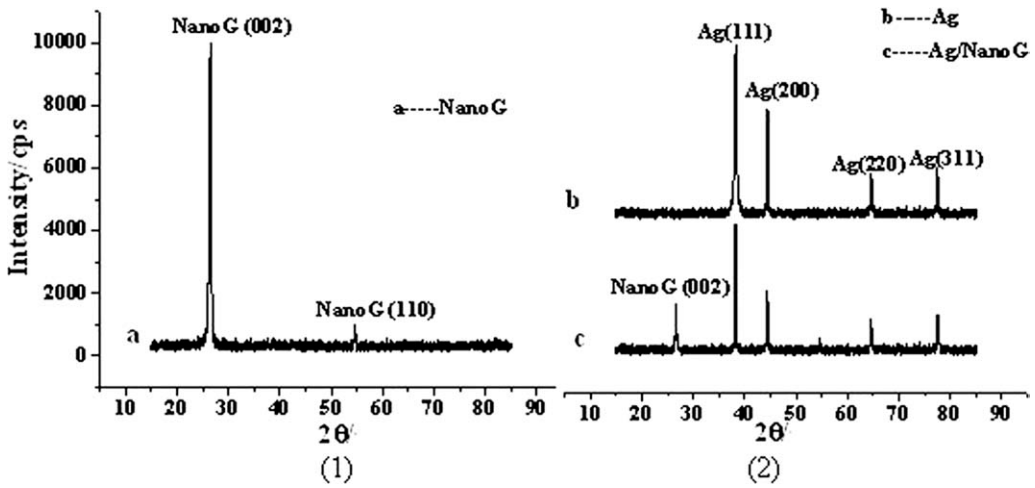

Figure 9 XRD curves of NanoG, Ag, and Ag/NanoG.

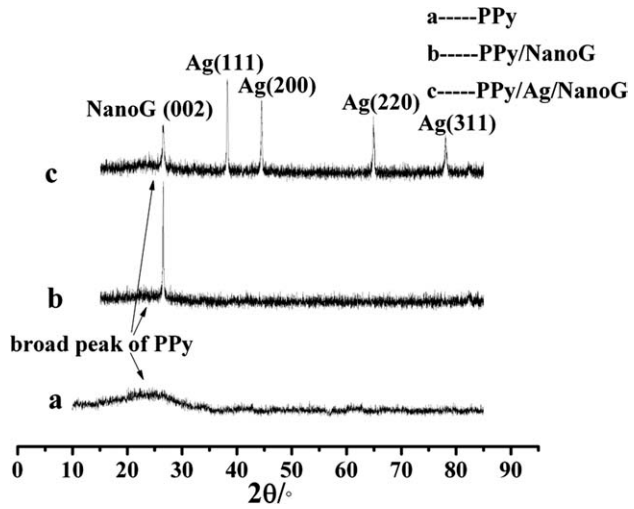

Figure 10 XRD curves of PPy, PPy/NanoG, and PPy/Ag/NanoG

a chemical band between PPy and the filler that could affect the vibration frequency of the atoms connected with them. All of the phenomena indicated that PPy was not merely covered by NanoG and Ag/NanoG; there were physical or chemical effects between PPy and the inorganic fillers.

Thermal analysis

To improve the stability of the polymers, they were always filled with inorganic fillers. In this study, NanoG and Ag/NanoG were used as the templates and were wrapped up by PPy. Figure 12 shows the TG curves of pure PPy, PPy/NanoG, and PPy/Ag/NanoG. From the TG curves, it can be seen that both pure PPy and the PPy/NanoG and PPy/Ag/NanoG nanocomposites showed only one decomposition peak. The previous 10% weight loss between 0 and

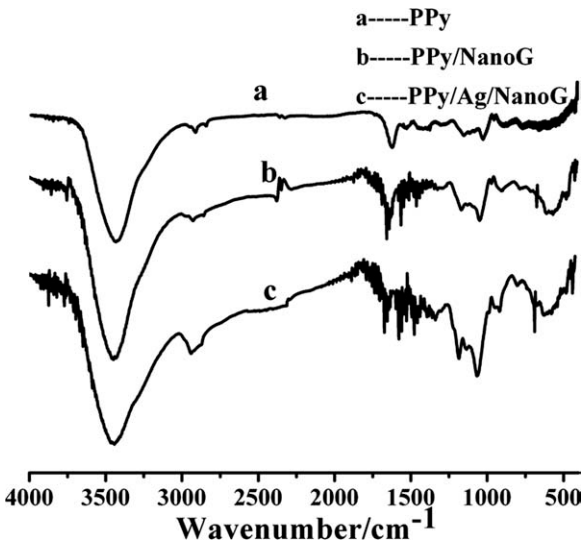

Figure 11 FTIR spectra of PPy, PPy/NanoG, and PPy/Ag/NanoG

TABLE II
FTIR Bands of PPy, PPy/NanoG, and PPy/Ag/NanoG

Wave number (cm^{-1})			
PPy	PPy/NanoG	PPy/Ag/NanoG	Functional group affiliation
3427	3438	3442	N—H stretching vibrations
1620	1633	1648	N—H in-plane deformation vibrations
1524	1554	1557	C—C stretching vibrations
1424	1442	1452	C—N stretching vibrations
1155	1160	1181	=C—H in-plane deformation vibrations
1022	1035	1038	N—H out-of-plane deformation vibrations
885	887	895	=C—H out-of-plane deformation vibrations

100°C resulted from the volatilization of the water in the samples. Then, the curves changed smoothly and level. Their degradation temperatures were about 300°C because of the pyrolysis of the main chain. The pure PPy had a residue of 21.80 wt % at 750°C, whereas the PPy/NanoG and PPy/Ag/NanoG nanocomposites had residues of about 30.37 and 53.88 wt %, respectively. The temperatures at different weight losses (20, 25, 30, and 35%) are shown in Table III. Data showed that all of the temperatures in the PPy/NanoG and PPy/Ag/NanoG curves were higher than those in the PPy curve; this indicated the enhanced thermal stability of the nanocomposites. The reason was that NanoG could impose restriction on the pyrolysis of the PPy chain and prevent heat concentration. This showed that there was a strong interaction among the large numbers of surface atoms of silver particles and NanoG and PPy molecule chains.

Electrical analysis

The conductivities of NanoG, Ag, Ag/NanoG, PPy and the PPy/NanoG, and PPy/Ag/NanoG

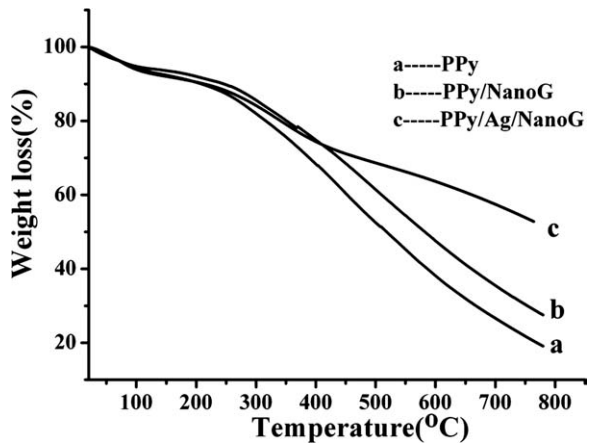

Figure 12 TG curves of PPy, PPy/NanoG, and PPy/Ag/NanoG

TABLE III
Temperatures (°C) at to Different Weight Losses

Sample	Weight loss (wt %)			
	20	25	30	35
Pure PPy	316.32	354.99	389.29	422.32
PPy/NanoG	351.10	398.84	438.90	475.27
PPy/Ag/NanoG	341.05	392.50	472.28	574.91

nanocomposites were measured with the SZ-82 digital four-probe resistance tester. The results are shown in Tables IV–VI. Table IV shows the conductivity values of NanoG, Ag, and Ag/NanoG. The conductivity value of NanoG could reach 9.06×10^3 S/cm; this indicated that NanoG was a good conductor. As an expensive metal, the conductivity value of Ag could reach 8.78×10^5 S/cm. After NanoG and Ag were assembled together, the conductivity value of Ag/NanoG was about 4.92×10^5 S/cm; this was higher than NanoG but lower than Ag. Wrapped up by Ag, the conductivity of NanoG could be enhanced prominently.

Figure 13 shows the conductivity value changes in the PPy/NanoG composite with different NanoG contents. The conductivity of the PPy/NanoG composite dramatically increased with increasing NanoG content. When the mass ratio of NanoG to PPy was 2.25%, the conductivity of the PPy/NanoG reached the maximum, that is, 5.15 S/cm. After that, with increasing of NanoG content, the conductivity of the PPy/NanoG still increased, but the pace of it changed slowly. The reason was that NanoG was well-dispersed in the composite and the conductive network could not be formed when the quantity of NanoG was low. In this circumstance, the conductivity of the composite was primarily from PPy. With a higher content of NanoG, its particles connected with each other, and some conductive networks were formed. These contributed to the conductivity of the composite. When the NanoG content reached a critical value, the partial networks contacted each other, and conductive passageways were formed. This led to a dramatic conductivity increase. After that, the conductivity value of the composite changed very slowly (Fig. 14).

The critical value of NanoG content in the composite was named the *percolation threshold* and was lower than those with carbon black or OG as filler. With a high aspect ratio (width-to-thickness ratio),

TABLE IV
Conductivity Values of NanoG, Ag, and Ag/NanoG (S/cm)

Sample	NanoG	Ag	Ag/NanoG
Conductivity value	9.06×10^3	8.78×10^5	4.92×10^5

TABLE V
Conductivity Values of PPy, PPy/NanoG, and PPy/Ag/NanoG (S/cm)

Sample	PPy	PPy/NanoG	PPy/Ag/NanoG
Conductivity value	0.52	5.15	156.34

the structure of NanoG in the polymer matrix was extremely beneficial to the formation of a conductive network. Thus, the conductivity of the polymer was enhanced in this way.

As to the PPy/Ag/NanoG composite, its conductivity value with an Ag/NanoG content of only 1.50 wt % was found to be 156.34S/cm; this was three orders of magnitude greater than that of pure PPy (0.52S/cm). The conductivity of the final PPy/Ag/NanoG composite dramatically increased compared with that of pure PPy; this indicated its possible use as an electromagnetic interference shielding material.

Microwave-absorbing properties

According to the absorbing mechanism, microwave-absorbing materials can be divided into two types, magnetic materials with the mechanism of magnetic loss and electronic materials with the mechanism of dielectric loss. The microwave-absorbing properties of materials can been expressed by the following parameters: complex permittivity ($\varepsilon^* = \varepsilon' - j\varepsilon''$), (where ε' refers to the real part of the complex permittivity and ε'' refers to the imaginary part of the complex permittivity) complex permeability ($\mu^* = \mu' - j\mu''$), (where μ' refers to the real part of the complex permeability, μ'' refers to the imaginary part of the complex permeability and j is the imaginary unit of the imaginary numbers) dielectric loss ($\tan \delta_e = \varepsilon''/\varepsilon'$), and magnetic loss ($\tan \delta_m = \mu''/\mu'$). The electromagnetic parameters of NanoG, Ag/NanoG, PPy, PPy/NanoG, and PPy/Ag/NanoG were measured. On the basis of the measured data, the microwave-absorbing properties of the obtained samples could be calculated and could be expressed by the reflection loss.

Figure 15 show the reflection losses of NanoG, Ag/NanoG, PPy, Ag/NanoG, and PPy/Ag/NanoG at different frequencies. The reflection loss of PPy was below −10 dB (90% absorption) at 9.2–12.4 GHz, and the minimum loss value was −12.09dB at 10.2 GHz. The bandwidth corresponding to the reflection loss below −10 dB was 3.2 GHz. For PPy/Ag/NanoG, the reflection loss was below −15 dB at

TABLE VI
Percolation Thresholds of NanoG and Ag/NanoG Used in the Composites (wt %)

Filler	NanoG	Ag/NanoG
Percolation threshold	2.25	1.50

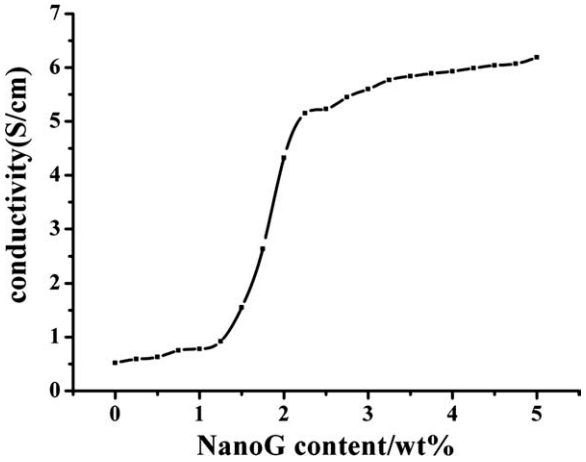

Figure 13 NanoG content in the PPy/NanoG composites.

an *X* band from 8.2 to 12.4 GHz, and the minimum loss value was −18.21 dB at 9.86 GHz. The bandwidth corresponding to the reflection loss below −15 dB was 4.2 GHz. To PPy/NanoG, the reflection loss was below −10 dB at an *X* band from 8.2 to 12.4 GHz, and the minimum loss value was −13.44 dB at 10.28 GHz. The bandwidth corresponding to the reflection loss below −10 dB was 4.2 GHz.

The absorbing mechanism of PPy was mainly dielectric loss. The high conductivities of NanoG and Ag/NanoG could improve the conductivity of PPy. At the same time, the high aspect ratios (width-to-thickness ratio) of NanoG and Ag/NanoG made PPy well dispersed, so the dielectric losses of PPy/NanoG and PPy/Ag/NanoG were higher than that of PPy, and their microwave-absorbing properties were superior to that of PPy.

CONCLUSIONS

In this article, nanocomposites PPy/NanoG and PPy/Ag/NanoG were fabricated via the *in situ* polymerization of Py in the presence of NanoG and Ag/NanoG. The morphologies and nanostructures of EG, NanoG, Ag/NanoG, PPy/NanoG, and PPy/Ag/NanoG were characterized by SEM, EDS, FTIR spectroscopy, and XRD. The results illustrate that NanoG had a great aspect ratio (width-to-thickness ratio) and could be chemically coated by Ag. Through *in situ* polymerization, most of the NanoG and Ag/NanoG nanoparticles could be encapsulated by PPy. The TG analysis suggested that with the introduction of inorganic nanosilver and NanoG, the composites exhibited better thermal stability than pure PPy. According to the four-point probe test, the conductivities of the ultimate PPy/NanoG and PPy/Ag/NanoG composites were dramatically increased compared with that of pure PPy. Measurements of the reflection loss showed that the microwave-absorbing properties of PPy/Ag/NanoG and PPy/NanoG were superior to that of PPy and should make possible their use as electromagnetic interference shielding materials.

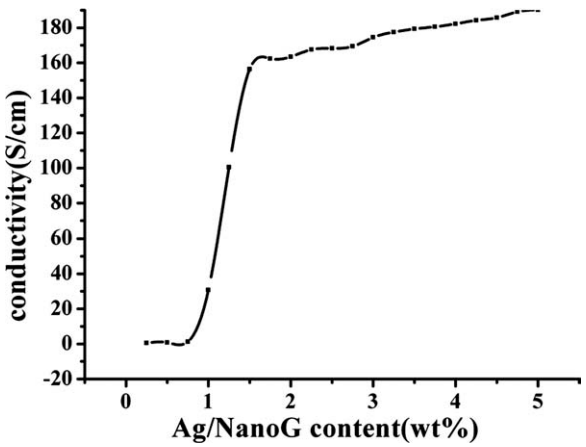

Figure 14 Ag/NanoG content in the PPy/Ag/NanoG composite.

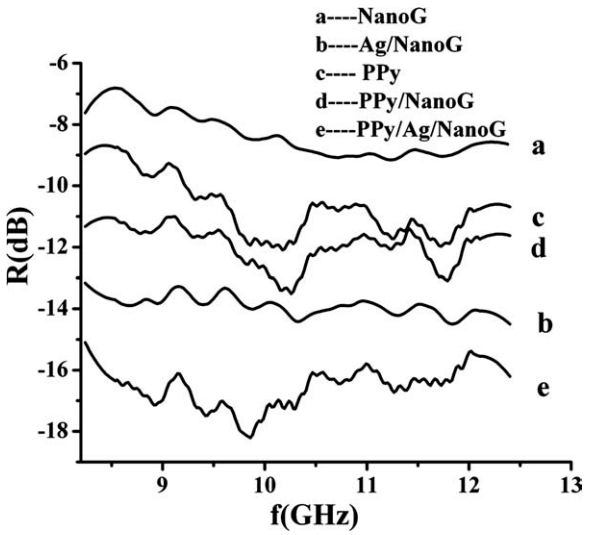

Figure 15 Reflection loss (*R*) of NanoG, Ag/NanoG, PPy, PPy/NanoG, PPy/Ag/NanoG, and f, frequency.

References

1. Wang, Y. P.; Li, L. C.; Jiang, J. React Funct Polym 2008, 68, 1587.
2. Zhong, T. B.; Hou, G. Y. Chem Mater 1999, 11, 1581.
3. Goh, S. H.; Chan, H. S. O.; Ong, C. H. J Appl Polym Sci 1998, 68, 1839.
4. Khan, M. A.; Armes, S. P. Adv Mater 2000, 12, 671.
5. Haldorai, Y.; Min, H. W.; Eun, J. P. Eur Polym J 2008, 44, 637.
6. Shen, Y. Q.; Wan, M. X. J Appl Polym Sci 1998, 68, 1277.
7. Jamshid, K.; Avlyanov, J. K. Synth Met 1999, 102, 1272.
8. Xue, P.; Tao, X. M. J Appl Polym Sci 2005, 98, 1844.
9. Saswata, B.; Tapas, K. L.; Uddin, M. E.; Kim, N. H.; Lau, A. K. T.; Lee, J. H. Polymer 2010, 51, 5921.
10. Fan, J. H.; Wan, M. X.; Zhu, D. B. J Appl Polym Sci 1999, 74, 2605.
11. Wu, X. M.; Qi, S. H.; He, J. J Mater Sci 2010, 45, 483.

12. Xiao, M.; Sun, L. Y.; Liu, J. J. Polym 2002, 43, 2245.
13. Parveen, S.; Veena, C.; Sood, K. N.; Dhawan, S. K. J Appl Polym Sci 2009, 113, 3146.
14. Zheng, G. H.; Wu, J. S.; Wang, W. P. Carbon 2004, 42, 2839.
15. Asma, Y.; Jyi-Jiin, L.; Isaac, M. D. Compos Sci Technol 2006, 66, 1182.
16. Xie, Y. C.; Yu, D. M.; Guo, X. S. J Appl Polym Sci 2009, 112, 3613.
17. Li, L. B.; An, M. Z. J Alloys Compd 2008, 461, 85.
18. Macauley, D. J.; Kelly, P. V.; Mongey, K. F. Appl Surf Sci 1991, 38, 622.
19. Tang, X. J.; Cao, M.; Bi, C. L. Mater Lett 2008, 202, 4868.
20. Zhang, Q. Y.; Wu, M.; Zhao, W. Scr Mater 2008, 59, 1031.
21. Jun, J. B.; Seo, M. S.; Cho, S. H. J Appl Polym Sci 2006, 100, 3801.
22. Li, Y. F.; He, G. F. Synth Met 1998, 94, 127.
23. Zheng, G. H.; Wu, J. S.; Wang, W. P. Carbon 2004, 42, 2839.
24. Chen, G. H.; Weng, W. G.; Wu, D. J. Carbon 2004, 42, 753.
25. Wu, X. M.; Qi, S. H.; He, J. J Polym Res 2009, 15, 660.
26. Yang, X. M.; Liang, L. Synth Met 2010, 160, 1822.
27. Xing, S. X.; Zhao, G. K. Mater Lett 2007, 61, 2040.
28. Zhao, C. J.; Zhao, Q. T.; Zhao, Q. Z. J Photochem Photobiol A 2007, 187, 146.
29. Wang, W. Q.; Li, W. L.; Zhang, R. F. Synth Met 2010, 160, 2255.
30. Jia, Q. M.; Shan, S. Y.; Jiang, L. H.; Wang, Y. M. J Appl Polym Sci 2010, 115, 26.